Nanoscale

COMMUNICATION

View Article Online
View Journal

A single electron nanomechanical Y-switch†

Chulki Kim,[a] Hyun-Seok Kim,*[b] Marta Prada[c] and Robert H. Blick[d]

Cite this: DOI: 10.1039/c4nr01298d

Received 9th March 2014
Accepted 23rd May 2014

DOI: 10.1039/c4nr01298d

www.rsc.org/nanoscale

We demonstrate current switching in the frequency domain using a nanomechanical shuttle with three terminals operating at room temperature. The shuttle consists of a metallic island on top of a Si nanopillar forming the Y-junction. A flexural mode of the nanopillar is excited by applying an external bias to one of the contacts, allowing electrons to be shuttled across the oscillating island.

The combination of nanomechanical resonators with single electron devices, so-called electron shuttles, is an extremely promising area within the larger field of nano-electromechanical systems (NEMS). With the continuing size reduction of NEMS circuits single electron devices can now be operated at room temperature.[1] It was shown before how two-junction nanomechanical shuttles can be operated in the radio frequency regime. The next step we discuss in this Letter is to investigate the applicability of three-junction shuttles, herein a so-called Y-junction. The advantage of such a nanomechanical Y-switch is essentially the strongly suppressed leakage current,[2] excelling CMOS-based switches as basic elements for few-electron logic applications with precise electron transfer. Y-switches have been extensively studied in semiconductor heterostructures, suggesting a new fashion for further miniaturization of the semiconductor based transistors.[3,4] Modulation of the current signals at GHz-speed[5] excels other lateral architectures.[6] In addition, NEMS switches have demonstrated superior characteristics such as operation in harsh environments or superior throughput insulation.[1,7–11] The recent experimental[12,13] and theoretical[14,15] findings have indeed opened a new vista on the realization of NEMS-based quantum information devices.

In this work we demonstrate tunable different mechanical modes in a NEMS-based Y-branch switch operating in the quantum mechanical limit at 300 K. We tune the mechanical modes by shifting the input frequency of the signal, allowing control of the current channel throughout the system. This approach based on the single electron shuttle suggests the realization of an ultra low-power logic element.

A scanning electron microscope image of the nanomechanical current switch is shown in Fig. 1(a). The silicon nanopillar has a height of 250 nm and the top gold layer has a

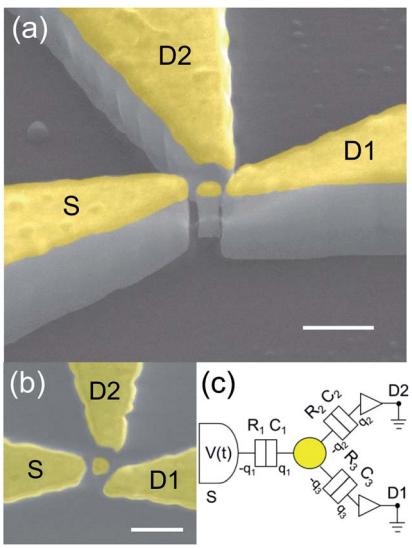

Fig. 1 (a) A scanning electron microscopy image of the nanomechanical Y-switch. The 250 nm height nanopillar is at the center and the gap distances towards source (S), drain-1 (D1), and drain-2 (D2) are 30, 21, and 50 nm, respectively. A gold layer (yellow) of 50 nm is thermally deposited. The scale bar indicates 200 nm. (b) Top view of three electrodes around the nanopillar. (c) Simplified circuit diagram of the nanopillar switch system. The metallic grain (center) is linked to three electrodes by mechanical modulation.

[a]Sensor System Research Center, Korea Institute of Science and Technology, 136791 Seoul, Republic of Korea

[b]Dongguk University-Seoul, 100715 Seoul, Republic of Korea. E-mail: hyunseokk@dongguk.edu

[c]I. Institut für Theoretische Physik, Universität Hamburg, Jungiusstr. 9, 20355 Hamburg, Germany

[d]Institut für Angewandte Physik, Universität Hamburg, Jungiusstr. 11, 20355 Hamburg, Germany

† Electronic supplementary information (ESI) available. See DOI: 10.1039/c4nr01298d

diameter of 70 nm. The gap distances towards the two electrodes (S and D1) are 30 nm and 21 nm. Another electrode (D2) is located farther away, with a gap distance of 50 nm. The top view of the nanomechanical Y-switch is shown in Fig. 1(b). The device is realized using standard clean room techniques and electron beam writing: first electrical contact pads for radio frequency (RF) signal probing are patterned on a Silicon-On-Insulator (SOI) substrate *via* optical lithography. The SOI serves as a template for the actual device containing a buried oxide layer (350 nm) that provides a sufficient device-to-substrate insulation for electron transport, which occurs only through the metallic thin film on top of the device. A polymethyl-methacrylate (PMMA) bilayer is then spin-coated on top of the SOI. The system is designed in such a fashion that the metallic island is placed at the center, in close proximity to all three electrodes. They are defined by an electron beam writer operating at 30 kV accelerating voltage (dosage is 160 μC cm^{-2}). A 50 nm gold layer with a 5 nm Cr layer for adhesion is then thermally evaporated followed by a lift-off process using acetone. After etching out the silicon layer around the patterns in a reactive ion etcher (UNAXIS 790 RIE), we obtain a single nanopillar surrounded by three electrodes. To ensure that the gold layer is the only conduction path for electrons, the substrate is etched down into the insulating layer. All measurements are performed using high frequency probes (DC to 50 GHz) under vacuum ($\leq 10^{-5}$ mbar) at room temperature. The DC measurement setup is schematically described in Fig. 1(c): The current flow is monitored *via* the electrodes (D1 and D2).

Fig. 2(a) shows the *I*–*V* curves along the two possible channels *via* the nanopillar. We label the involved channels as Ch1 for S-D1 current and Ch2 for S-D2 current, as depicted in the corresponding insets of Fig. 2(c) and (d). The currents through Ch1 and Ch2 are plotted in a Fowler–Nordheim manner in Fig. 2(b). The positive slope unlike the conventional Fowler–Nordheim curve indicates that the current for the low voltages is dominated by the AC field rather than the DC field as discussed in ref. 16. The system behaves as an asymmetric triple junction, where mechanically assisted tunneling is the dominant electron transfer mechanism. The step-like structure reveals Coulomb blockade (CB)[1,17] in an asymmetric configuration. The CB plateaus for the S-D1 electron transfer (~200 mV) are larger than those for the S-D2 (~60 mV). To match with the experiment, we express the free energy for the left to right tunneling event $\vec{\mu}^i$ ($i = 1$, 2, and 3 labels the junction, see Fig. 1) in terms of the bias,[18,19]

$$\vec{\mu}^i = \frac{e}{C_\Sigma}\left[e\left(\frac{1}{2} \pm n\right) - V\sum_{j\neq i} C_j(x)\right], \qquad (1)$$

where we defined $C_\Sigma = \sum_i C_i$ and C_i depends on the deflection of the island, x: $C_1 \simeq C_1^0/(1+x)$, $C_2 \simeq C_2^0/(1-x)$, and $C_3 \simeq C_3^0/(1-x)$ with $|x| < 1$ (we express x in units of the junction width) and the static capacitances, C_i^0. The criterion for tunneling is that the free energy given by eqn (1) is lowered, $\vec{\mu}^i < 0$. This involves the term in brackets to be negative, defining a position-dependent CB threshold voltage, V^{th}. Assuming the flexural mode sketched in the insets of Fig. 2 (blue double-headed arrow) and that the tunneling events occur at the points of maximal deflection, $x = x_0$ (note that the resistance depends exponentially on the distance to the contact), two threshold voltages can be defined,

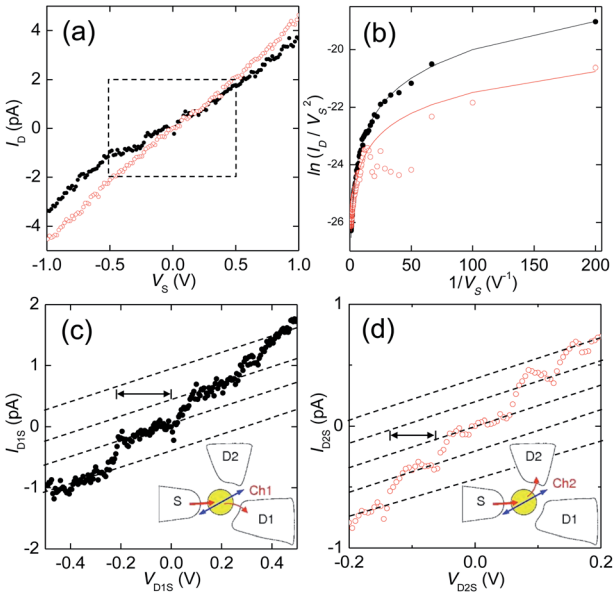

Fig. 2 (a) Currents across Ch1 (black), involving S and D1 electrodes, and Ch2 (red), involving S and D2 electrodes. (b) Currents through Ch1 and Ch2 at different voltages plotted in a Fowler–Nordheim representation. They are well fitted by considering the time-averaged tunneling current.[16] The boxed region in (a) is magnified in (c) and (d). A stepwise current increase by Coulomb interaction is observed in both channels at room temperature. The dashed lines guide the Coulomb staircase. The charging energies for both channels indicated by arrows are much larger than the thermal energy at room temperature of 26 meV.

$$V_{\mathrm{D1}}^{\mathrm{th}} \simeq \frac{e}{2[C_1^0 + C_2^0 - x_0(C_1^0 - C_2^0)]}(1 - x_0^2);$$

$$V_{\mathrm{D2}}^{\mathrm{th}} \simeq \frac{e}{2[C_1^0 + C_3^0 - x_0(C_1^0 - C_3^0)]}(1 - x_0^2).$$

Fig. 1 suggests $C_1^0 \sim C_3^0 \gg C_2^0$. We take $C_{1,3}^0 = C$ and $C_2^0 = \alpha C$. Using the results of Fig. 2, we extract the plateau ratio, $V_{\mathrm{D2}}^{\mathrm{th}}/V_{\mathrm{D1}}^{\mathrm{th}} \sim 0.3$, giving $x_0 \simeq 0.75$ for $\alpha \sim 0.2$, and $C \sim 0.8$ aF.

We now proceed to explore the mechanical clocking of our device by applying a time-dependent voltage. The dynamics of the shuttle can be described in terms of a mechanical oscillator subject to a force given by the time varying electrostatic field,[20]

$$\ddot{x} = -\gamma\dot{x}(t) - \omega_0^2 x(t) - \frac{\tilde{q}(t)V(t)}{mL}, \qquad (2)$$

where m is the mass of the electron shuttle, ω_0 is the oscillator eigenfrequency, γ is the damping coefficient, L is the distance between two electrodes and $\tilde{q}$ is related to the excess charge on the nanoislands. We stress that the latter quantity depends in turn on x, resulting in nonlinearities. Finite-element simulation

software[21] allows us to estimate the fundamental mode at $\omega_0 \simeq$ 440 MHz. Eqn (2) is known to have resonant modes[17] when the excitation $V(t) = V_0 \cos \omega t$ has a frequency ω commensurate with the fundamental mode frequency, ω_0, *i.e.*, $\omega = (p/q)\omega_0$ with p and q being integers, or in other words, the motion of the shuttle is synchronized with the signal, such that for every p periods of the oscillating excitation, the shuttle performs q oscillations. This effect is commonly termed as mode-locking.[20,22,23]

We monitor the mechanical response of our system by sweeping a radio frequency signal in the range of 400 MHz to 1 GHz. Fig. 3(a) shows the response in terms of direct current through either channel, Ch1 or Ch2, at the signal power of 16.5 dBm (see also Fig. S1†). The magnitude of the currents measured throughout this work (~pA) reveals that the shuttle does not operate in the self-excitation regime.[1] The current spectrum also reflects that different mechanical modes of the nanopillar are excited on subsequent frequency ranges, activating all possible electron transport channel combinations. We label the super-harmonics with the corresponding p/q values in Fig. 3(a). The switching response of Ch1 is summarized in Fig. 3(b), assuming an upper (ON) and lower (OFF) threshold currents of 10 and 90% of the maximum peak, respectively. When driven by radiofrequency signals, we observe in the time-domain that Ch1 is active at 440 MHz and inactive at 800 MHz as demonstrated in Fig. 3(c). It is worth noting the two large current spikes in the signal, appearing on both sides of the input pulse (only partially shown). These are due to the effective capacitance of the island. The width at the resonances suggests a Q-factor of 5–20 as indicated by arrows at 440 MHz and 800 MHz (see Fig. 3(a)), involving a ring-down time of a few nanoseconds. The enhanced current peaks at around 440 MHz indicate that, in the corresponding active mode, the tunneling distance from the island to either drain is similar in the maximal deflection of the flexural mode. Finite element simulation[21] shows indeed a mode activating both channels in Fig. 3(d). However, in the yellow-shaded region ($450 < f < 597$ MHz) of Fig. 3(a) and (b), the current towards D2 is suppressed and occurs mainly *via* D1, allowing only channel Ch1. In contrast, the current occurs mainly *via* D2 over the red-shaded region (>597 MHz), activating channel Ch2. The corresponding finite element simulation for the modes activating Ch1 and Ch2 is presented in Fig. 3(e) and (f). Structural analysis allows the flexural, longitudinal, and torsional modes of the nanopillar. Fig. 3(d–f) depict the active channel on each mode by coupling structural analysis with an electric potential distribution upon mechanical oscillation. The fundamental mechanical mode, which is a flexural shape as shown in Fig. 3(d), corresponds to $p/q = 1$, and Fig. 3(e) and (f) correspond to $p/q = 5/4$ and $9/5$, respectively. The one for $p/q = 5/4$ next to the fundamental mode shows also a similar flexural mode. However, coupling of flexural and torsional motions is obtained for $p/q = 9/5$ as shown in Fig. 3(f). The upper color scale in Fig. 3(d–f) represents an electric potential across the Y-switch with the application of an AC signal at 16.5 dBm and the bottom one indicates the range of displacement in motion. The insets of Fig. 3(d–f) depict schematically the active channel in each mode.

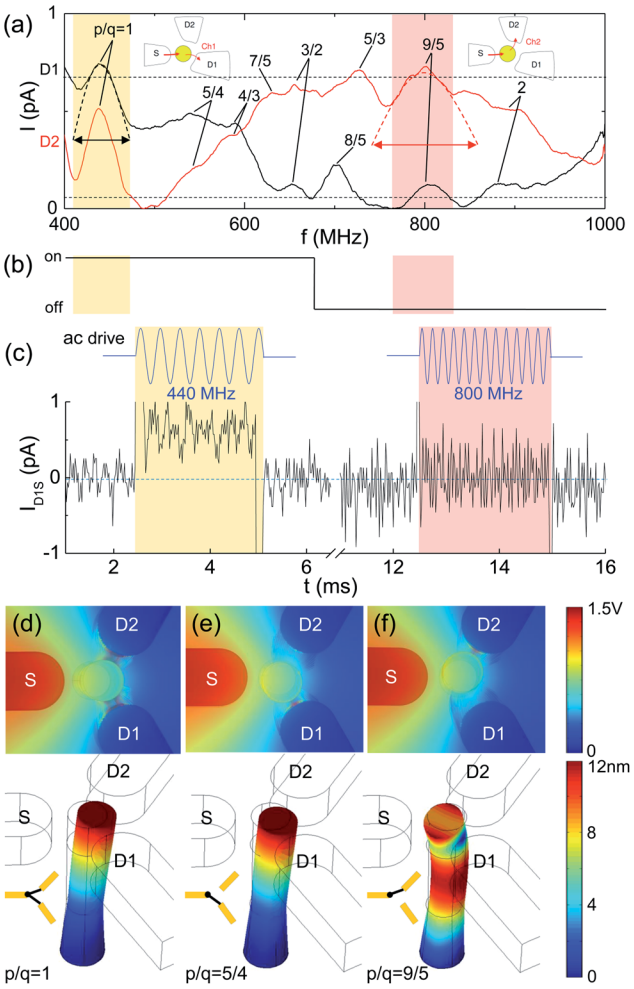

Fig. 3 (a) Current *vs.* frequency traces measured at D1 (black) and D2 (red) with the labels of the corresponding p/q values. (b) Switching response of Ch1 with the assumption of an upper (ON) and lower (OFF) threshold currents of 10 and 90% of the maximum peak. (c) Output currents in a time-domain with the application of radiofrequency signals at 440 MHz and 800 MHz. Ch1 is active at 440 MHz and inactive at 800 MHz with the corresponding input signals. (d) Finite element calculation on an electric potential distribution (upper) and mechanical modes (lower) of the nanomechanical Y-switch. Charge transport relies on mechanical clocking where the nanopillar oscillates between electrodes due to an applied AC signal at the source electrode (S). Electrons tunnel into D1 and D2 electrodes at their fundamental resonant mechanical response of 440 MHz, activating both Ch1 and Ch2. (e) Mechanical mode activating Ch1 dominantly. (f) Mechanical mode activating Ch2 dominantly.

As demonstrated above, the electron shuttle plays the role of a mechanical switch, providing the capability of activating different channel combinations by shifting the input frequency. This gives rise to a variety of switching applications, such as frequency dependent RF switches, band pass filters, and various logic elements with different switch combinations.[24] In what follows, we propose an XOR gate consisting of two coupled nanomechanical switches as depicted in Fig. 4. When no channel is active, we have an open circuit. On active channel operation, the equivalent circuit of each switch corresponds to a resistance (R_{SD1}, R_{SD2}) in parallel with the capacitance

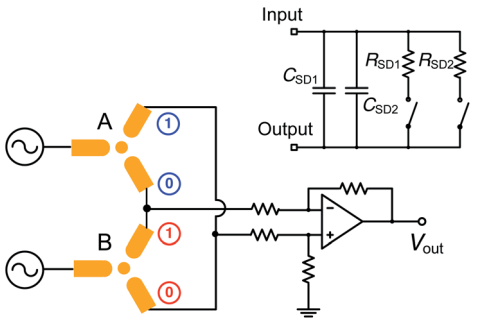

Fig. 4 A logic element model: the XOR gate can be constructed from two sets of the nanomechanical switch which are modulated by input frequencies. The upper inset shows an effective equivalent for the nanomechanical switch using a switched-capacitor model. The output is high if the two inputs (A and B) are not alike, otherwise the output is low.

(C_{SD1}, C_{SD2}) as shown in the upper inset of Fig. 4. The average current is given by $I^{i}_{ave} = (V(t)/2R_{SDi})(\Delta t/T)$, where $i = 1, 2$, $V(t)$ is the time dependent input voltage, and $\Delta t/T$ is the duty cycle, with Δt being the effective contact time.[25] On a channel-activating mechanical mode, the effective resistance is $R_{eff} = 2R_{SDi}(T/\Delta t)$. The output currents from both switches (A and B) are delivered towards the op-amp. Note that the op-amp can be realized by NEMS switches as well.[24] A high output from the op-amp occurs only if both switches oscillate at different frequencies and activate different channels. This corresponds to different logic inputs such as (1, 0), when Ch2 is active in A and Ch1 is active in B or (0, 1), when Ch2 is active in B with Ch1 being active in A. If both switches oscillate in the same mode, the output is low. A nanomechanical switch such as the one presented here offers great potential especially in realizing ultra low-power consumption logic elements thanks to mechanically assisted electron tunneling.

In general, resonators based on nanomechanical beams present an impressive quality factor over a wide temperature range, but frequently require cryogenics for Coulomb-controlled charge transfer, being limited by the operating conditions and ring-down times. In contrast, the vertical oscillator presented here with a moderate Q-factor allows shifting the active channel in the frequency domain as well as controlling electron transport with the extreme accuracy at room temperature.

In conclusion, we presented a nanopillar coupled to three contacts, showing mechanically assisted electronic current. Coulomb blockade enhanced steps were visible at room temperature, even in the absence of an AC signal. The mechanical clocking of the system was studied by monitoring the output current in the frequency domain. We found that we were able to control the current channel by shifting the input frequency, a key element for the realization of an ultra small current switch. Based on this switching property, an ultra low-power logic element (an XOR gate) model is suggested.

Acknowledgements

This work was partly supported by the DARPA NEMS-CMOS program (N66001-07-1-2046), the KIST Institutional program (2V03390), the KIST Future Fundamental Research Program, and the Electronics and Telecommunications Research Institute.

References

1 C. Kim, M. Prada and R. H. Blick, *ACS Nano*, 2012, **6**, 65.
2 J. E. Jang, S. N. Cha, Y. J. Choi, D. J. Kang and T. P. Butler, *Nat. Nanotechnol.*, 2008, **3**, 26.
3 L. Worschech, B. Weidner, S. Reitzenstein and A. Forchel, *Appl. Phys. Lett.*, 2001, **78**, 3325.
4 S. Reitzenstein, L. Worschech, P. Hartmann, M. Kamp and A. Forchel, *Phys. Rev. Lett.*, 2002, **89**, 226804.
5 M. D. Blumenthal, B. Kaestner, L. Li, S. Giblin, T. J. B. M. Janssen, M. Pepper, D. Anderson, G. Jones and D. A. Ritchie, *Nat. Phys.*, 2007, **3**, 343.
6 S. C. Masmanidis, R. B. Karabalin, I. De Vlaminck, G. Borghs, M. R. Freeman and M. L. Roukes, *Science*, 2007, **317**, 780.
7 T.-H. Lee, S. Bhunia and M. Mehregany, *Science*, 2010, **329**, 1316.
8 D. V. Scheible and R. H. Blick, *Appl. Phys. Lett.*, 2004, **84**, 4632.
9 H. S. Kim, H. Qin and R. H. Blick, *Appl. Phys. Lett.*, 2007, **91**, 143101.
10 H. S. Kim, H. Qin and R. H. Blick, *New J. Phys.*, 2010, **12**, 033008.
11 C. Kim, J. Park and R. H. Blick, *Phys. Rev. Lett.*, 2010, **105**, 067204.
12 H. Okamoto, A. Gourgout, C.-Y. Chang, K. Onomitsu, I. Mahboob, E. I. Chang and H. Yamaguchi, *Nat. Phys.*, 2013, **9**, 480.
13 T. Faust, J. Rieger, M. Seitner, J. Kotthaus and E. Weig, *Nat. Phys.*, 2013, **9**, 485.
14 K. Stannigel, P. Komar, S. J. M. Habraken, S. D. Bennett, M. D. Lukin, P. Zoller and P. Rabl, *Phys. Rev. Lett.*, 2012, **109**, 013603.
15 S. Rips and M. J. Hartmann, *Phys. Rev. Lett.*, 2013, **110**, 120503.
16 H. S. Kim, H. Qin, M. S. Westphall, L. M. Smith and R. H. Blick, *Nanotechnology*, 2007, **18**, 065201.
17 L. Y. Gorelik, A. Isacsson, M. V. Voinova, B. Kasemo, R. I. Shekhter and M. Jonson, *Phys. Rev. Lett.*, 1998, **80**, 4526.
18 M. Prada and G. Platero, *Phys. Rev. B: Condens. Matter Mater. Phys.*, 2012, **86**, 165424.
19 T. Nord, L. Y. Gorelik, R. I. Shekhter and M. Jonson, *Phys. Rev. B: Condens. Matter Mater. Phys.*, 2002, **65**, 165312.
20 F. Pistolesi and R. Fazio, *Phys. Rev. Lett.*, 2005, **94**, 036806.
21 *COMSOL, ver. 4.3b*, Burlington, MA, USA, 2013.
22 D. V. Scheible and R. H. Blick, *New J. Phys.*, 2010, **12**, 023019.
23 R. C. Hilborn, *Chaos and Nonlinear Dynamics*, Oxford University Press, New York, 2000.
24 R. H. Blick, H. Qin, H. S. Kim and R. A. Marsland, *New J. Phys.*, 2007, **9**, 241.
25 C. Weiss and W. Zwerger, *Europhys. Lett.*, 1999, **47**, 97.

